Continuous flow synthesis of bimetallic AuPd catalysts for the selective oxidation of 5-hydroxymethylfurfural to 2,5-furandicarboxylic acid

Stefano Cattaneo*,[a][b] Danilo Bonincontro,[c] Takudzwa Bere,[a] Christopher J. Kiely,[a][d] Graham J. Hutchings,[a] Nikolaos Dimitratos[a][c] and Stefania Albonetti*[c]

Abstract: The production of 2,5-furandicarboxylic acid (FDCA) from the selective oxidation of 5-hydroxymethylfurfural (HMF) is a critical step in the production of biopolymers from biomass-derived materials. In this study, we report the catalytic performance of monometallic Au and Pd, and bimetallic AuPd nanoparticles with different Au:Pd molar ratios synthesised under continuous flow conditions using a millifluidic set-up and subsequently deposited onto titanium dioxide as the chosen support. This synthetic technique provided a better control over mean particle size and metal alloy composition, that resulted in higher FDCA yield when the catalysts were compared to similar batch-synthesised materials. A 99 % FDCA yield was obtained with the millifluidic-prepared AuPd/TiO_2 catalyst (Au:Pd molar composition of 75:25) after being calcined and reduced at 200 °C. The heat treatment caused a partial removal of the protective ligand (polyvinyl alcohol) encapsulating the nanoparticles and so induced stronger metal-support interactions. The catalyst reusability was also tested, and showed limited particle sintering after five reaction cycles.

.

[a] Dr. S. Cattaneo, T. Bere, Prof. C. J. Kiely, Prof. G. J. Hutchings and Prof. N. Dimitratos
Cardiff Catalysis Institute, School of Chemistry
Cardiff University
CF10 3AT, Cardiff, UK
E-mail: Stefano.Cattaneo2@unimi.it
BereT@cardiff.ac.uk
Chk5@lehigh.edu
Hutch@cardiff.ac.uk
Nikolaos.Dimitratos@unibo.it

[b] Dr. S. Cattaneo
Dipartimento di Chimica
Università degli Studi di Milano
Via Golgi 19
20133, Milano, Italy

[c] Dr. D. Bonincontro, Prof. S. Albonetti, Prof. N. Dimitratos
"Toso Montanari" Department of Industrial Chemistry
University of Bologna
Viale Risorgimento 4
40136, Bologna, Italy
E-mail: Danilo.Bonincontro@unibo.it
Stefania.Albonetti@unibo.it
Nikolaos.Dimitratos@unibo.it

[d] Prof. C. J. Kiely
Department of Materials Science and Engineering
Lehigh University
5 East Packer Avenue
Bethlehem, Pennsylvania, PA 18015, USA

Supporting information for this article is given via a link at the end of the document.

Introduction

According to a recent statistical review of world energy published in 2018, 239 billion tons of proven crude oil reserves remain globally;[1] with a consumption of 4.6 billion tons per year (data referred to June 2017), the global oil reserves are expected to be depleted in less than 50 years. It is therefore crucial to find new viable renewable resources in order to reach both economic and environmental sustainability. Biomass, that is defined as material produced by the growth of microorganisms, plants or animals, has recently emerged as a promising alternative to fossil fuels. As the global population continues to rise, however, issues of food security must also be taken into consideration,[2] hence the need for the derivation of biomass from non-cultivable land and non-edible raw materials such as lignocellulose.[3–5]

Lignocellulose is mainly composed of cellulose, hemicellulose and lignin, and it currently represents *ca.* 75 % of the overall biomass production per year by photosynthesis (127 billion tons).[6] Amongst all the products derived from lignocellulosic biomass, 5-hydroxymethylfurfural (HMF) has recently captured the attention of both the academic and industrial world.[7,8] The simultaneous presence of a carbonyl and hydroxymethyl group directly attached to the aromatic furan ring, makes this renewable platform extremely versatile as well as an ideal starting point for the synthesis of several chemicals and biofuels.[9–12] The aerobic oxidation of HMF, in particular, leads to the formation of several kinds of important furanic chemicals, such as maleic anhydride (MA), 2,5-diformylfuran (DFF), 5-hydroxymethyl-2-furancarboxylic acid (HMFCA) and 2,5-furandicarboxylic acid (FDCA). Among all these products, the U.S. Department of Energy has listed FDCA as one of the top 12 value-added chemicals that can be derived from biomass.[13] FDCA, in fact, is a promising renewable alternative to the petroleum-derived terephthalic acid, a monomer widely used in the production of industrially relevant polyesters, such as polyethylene terephthalate (PET).[14] World polymer resin production almost reached 350 million tonnes in 2017, with PET currently representing about 10 % of the global plastic being generated. As a result, various companies have taken measures towards moving to more sustainable and renewable packaging, including Avantium that has developed a process that utilises FDCA for the synthesis of polyethylenefuranoate (PEF).[15]

The oxidation of HMF to FDCA was carried out in previous decades by using stoichiometric amounts of oxidants, such as $KMnO_4$, or homogeneous metal salts (mostly Co- and Mn-based).[16,17] Along with low selectivity and the high cost of the oxidants, these methods generated large amounts of toxic waste. A more environmentally friendly way to produce FDCA is by the selective oxidation of HMF with molecular oxygen; this reaction is typically carried out in water as solvent and it is catalysed by heterogeneous catalysts, particularly by supported noble metal

nanoparticles.[18–22] Ru-, Pt- and Pd-based catalysts have all shown high performance in both activity and selectivity towards the desired product, although these catalysts have often shown poor stability against deactivation, particularly with respect to oxygen poisoning and metal leaching.[23–27] Au-based catalysts have recently attracted attention in the aerobic oxidation of organic compounds due to their superior stability to water and oxygen compared with conventional liquid-phase oxidation catalysts.[28] Despite good activity and selectivity, however, Au nanoparticles are more prone to deactivation by adsorption of organic products or intermediates such as carboxylic acids.[29,30] The combination of Au with another noble metal (such as Pd, Pt or Ru) to form alloy nanoparticles may combine the advantages of the two components and therefore result in a highly active, selective and stable catalyst. The synergistic effect between Au and Pd, in particular, has proven to be very effective in several oxidation reactions, and it has been recently demonstrated for the oxidation of HMF to FDCA as well.[28,31–35] The chemical and physical properties of the bimetallic nanoparticles, however, play a crucial role in tuning the activity and selectivity towards the desired product. Small Au and Pd nanoparticles in the range of 2-5 nm, in fact, proved to be more active in this specific reaction.[36] Moreover, the concentration of the metals at the nanoparticle surface is not always the same as the nominal bulk composition and the surface composition can be strongly affected by the technique used for synthesis of the catalyst material.[37–39]

The control over the chemical and physical properties of bimetallic nanoparticles has long been a challenge. In a recent publication, however, we reported an innovative technique for the synthesis of supported bimetallic AuPd nanoparticles with exquisite control over both particle size and particle-to-particle composition.[40] The same experimental set-up was used for the synthesis of the bimetallic AuPd nanoparticles for exploiting the enhanced mixing properties of a millifluidic reactor and finally allowing nanoscopic control over the reaction conditions.

In this work, monometallic Au and Pd, and bimetallic AuPd nanoparticles with different Au:Pd molar ratios (namely 25:75, 50:50 and 75:25) were synthesised and deposited onto titanium dioxide using the millifluidic approach. TiO_2 was chosen as the support since recent studies showed remarkable activity and stability of TiO_2-based catalysts in the studied reaction.[41,42] The catalysts were then tested in the selective HMF oxidation in order to investigate the effect of the metal composition on the activity and selectivity to FDCA. The efficacy of the continuous synthesis technique was also evaluated by comparing the catalysts with their batch-synthesised counterparts. The effect of thermal treatment was also studied through a series of oxidation-reduction steps at different temperatures, ranging from 200 °C up to 400 °C since it is well known that the partial or complete removal of the ligand and the enhancement of metal-support interaction can improve activity, yield to desired products and long-term catalyst stability. Finally, the most active and selective catalyst was tested in consecutive reactions in order to evaluate the stability under the reaction conditions used.

Results and Discussion

Catalyst synthesis

Batch synthesis - The synthetic procedure used for this study and referred as “batch synthesis” is a protocol based on the Brust-Schiffrin method[43] and then further developed by Prati and coworkers.[44,45] This method involves the reduction of a metal salt ($HAuCl_4$ and/or K_2PdCl_4) dissolved in H_2O by a strong reducing agent ($NaBH_4$) in the presence of a stabilising agent (poly (vinyl alcohol) - PVA). The role of the stabilising agent is to protect the newly formed nanoparticles from agglomeration and coalescence by forming a protective surface layer. Once the colloid is prepared, the support is added (TiO_2) in order to immobilise the nanoparticles onto its surface.

Continuous synthesis - A scheme of the experimental setup used to produce supported Au, Pd and AuPd nanoparticles in continuous flow is reported in Figure S1. From now on it will be referred as “continuous synthesis”. The setup consists of a dual-channel peristaltic pump, a reactor (composed of a T-shape connection and tubing) and a glass container for the immobilisation of the colloid. One solution containing the metal precursors ($HAuCl_4$ and/or K_2PdCl_4) and the stabilising agent (PVA) and a second solution containing the reducing agent are pumped into the reactor by the peristaltic pump. The colloid produced then drops into a beaker containing the support (TiO_2) stirred in an acidified water solution. All the reaction parameters were kept similar to the batch protocol for a suitable comparison (see Experimental Section). The whole setup was kept at a constant room temperature of 25 °C.

Catalyst characterisation

Transmission electron microscopy analysis (TEM) was performed on all the samples in order to evaluate average particle size and particle size distribution. Representative TEM micrographs are presented in the Supplementary Information (Figures S2 and S3), along with the corresponding particle size distribution histograms. The average metal nanoparticle size was in the 3-5 nm range for the batch-synthesised catalysts and in the 2-4 nm range for those prepared using the continuous-flow set-up. This difference in particle size between the two preparation methods, highlighted in Table 1, has already been reported in a previous study and was attributed to a better mixing of the metal precursors with the reducing agent during particle formation.[40] The improved control over the reaction conditions was also shown to be responsible for a more uniform particle-to-particle chemical composition for the Au:Pd catalyst with molar ratio of 50:50.[40] X-ray photoelectron spectroscopy (XPS) analysis, in addition, suggests Au segregation, although in small extent, on the particle surface of the batch-synthesised catalysts (Table 2). On the other hand, with the continuous method, the metal composition is uniform all throughout the nanoparticle particle range.

Catalyst	Mean particle size (nm)	
	Batch method	*Continuous flow*
Au/TiO_2	4.5 ± 1.3	3.2 ± 0.9
$Au_{75}Pd_{25}/TiO_2$	3.7 ± 1.1	2.7 ± 0.7
$Au_{50}Pd_{50}/TiO_2$	3.0 ± 1.0	2.0 ± 0.7
$Au_{25}Pd_{75}/TiO_2$	3.1 ± 1.1	2.3 ± 0.8
Pd/TiO_2	4.6 ± 1.3	3.1 ± 1.0

Table 1. Particle size distribution of the monometallic Au and Pd and Au_xPd_y bimetallic catalysts prepared via the batch and continuous methods.

XPS analysis facilitated also in the identification of the Au and Pd oxidation state (Figure S6-S9). The $Au4f_{7/2}$ peak confirmed the presence of Au in the metallic state for the whole series of catalysts, with binding energy (BE) between 83.0 and 83.7 eV (Table 2).[46] In particular, the binding energies (BE) of the monometallic Au catalysts were 83.5 and 83.7 eV for the batch and continuous variants, respectively. These values are lower than the typical BE of bulk Au (ca. 84.0 eV), due to particle size effects and the presence of negatively charged Au species ($Au^{\delta-}$).[47] The BE of Au in the bimetallic catalysts further decreased due to electronic interactions between the two metals, confirming the presence of an alloy structure.[48] The analysis of the $Pd3d_{5/2}$ peak revealed the presence of both Pd^0 (*ca.* 334.9 eV) as the major species and Pd^{2+} species (*ca.* 337.0 eV), the latter attributed to PdO since no chloride was detected (Table 2). It is also interesting to notice that the continuous flow method consistently led to a higher Pd^0/Pd^{2+} ratio compared to the batch -synthesised catalysts.

Catalytic test results

The hydrogenation of HMF to FDCA takes place via a series of consecutive reactions (Figure 1). Typically, in the presence of a base, the first step is the oxidation of the carbonyl group to produce the carboxylic acid (5-hydroxymethyl-2-furancarboxylic acid, HMFCA). Further oxidation of this intermediate leads to 5-formyl-2-furancarboxylic acid (FFCA) initially and then FDCA. The production of 2,5-diformylfuran (DFF) is also sometimes reported, mainly in the absence of a base or with non-Au based catalysts.[34]

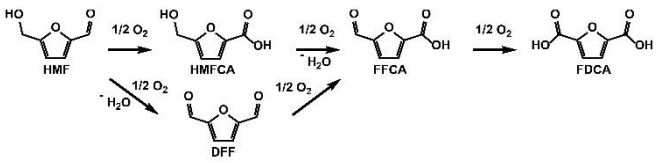

Figure 1. Reaction scheme of the HMF oxidation to FDCA.

From a previous study, bimetallic AuPd catalysts showed the highest selectivity to FDCA with a Au-rich composition.[32] For this reason, a first catalytic test was conducted with the bimetallic $Au_{75}Pd_{25}/TiO_2$-C catalyst (prepared using the continuous millifluidic set-up), in order to gain information on the reaction network. From TEM analysis, the catalyst showed an average particle size of 2.7 nm, with a particle size distribution of ± 0.7 nm (Figure 2 and Table 1). In addition, both XPS and ICP analyses confirmed the nominal Au:Pd molar ratio of 75:25 (Table 2).

The reaction (Figure 3) was conducted at 70 °C and 10 bar of O_2, using NaOH as base (NaOH/HMF molar ratio of 2). During the induction time (*i.e.* the time interval prior to reaching the set point temperature), HMF was entirely converted into HMFCA and FDCA (with 53 % and 27 % yields respectively). No FFCA was detected in the reaction mixture, meaning that the oxidation step from FFCA to FDCA was extremely fast. In addition, DFF was absent from the products, confirming that under these reaction conditions and with the catalyst used, the preferred pathway is through formation of HMFCA. Upon increasing the reaction time, the HMFCA converted into FDCA, reaching a final yield of 92 % after 4 h. At the same time, the unidentified products (represented as "Others" in Figure 3) decreased from 20 % yield at 0 min to 3 % yield after 4 h. Considering this trend in yield of the undefined products, and in light of the poor HMF stability under strong basic aqueous conditions, we suggest that these undefined products come from the degradation of unreacted HMF, which undergoes

Catalyst	Metal loading (wt%)	Au:Pd ratio (mol/mol)		Pd^0/Pd^{2+} (mol/mol)	Binding Energy (eV)	
	MP-AES	MP-AES	XPS	XPS	Au $4f_{7/2}$	Pd $3d_{5/2}$
Au/TiO_2-B	1.01	100 : 0	100 : 0	-	83.5	-
$Au_{75}Pd_{25}/TiO_2$-B	1.01	76 : 24	79 : 21	1.2	83.4	335.0
$Au_{50}Pd_{50}/TiO_2$-B	1.02	52 : 48	55 : 45	1.1	83.3	334.9
$Au_{25}Pd_{75}/TiO_2$-B	1.02	28 : 72	32 : 68	2.2	83.3	335.0
Pd/TiO_2-B	0.98	0 : 100	0 : 100	5.2	-	334.7
Au/TiO_2-C	1.00	100 : 0	100 : 0	-	83.7	-
$Au_{75}Pd_{25}/TiO_2$-C	0.99	75 : 25	76 : 24	2.2	83.2	334.7
$Au_{50}Pd_{50}/TiO_2$-C	0.99	52 : 48	51 : 49	2.1	83.0	334.7
$Au_{25}Pd_{75}/TiO_2$-C	1.00	26 : 74	23 : 77	2.2	83.2	334.8
Pd/TiO_2-C	0.98	0 : 100	0 : 100	5.7	-	334.8

Table 2. Metal loading, Au:Pd molar ratio and Pd^0:Pd^{2+} molar ratio of the catalysts prepared in batch (Au_xPd_y/TiO_2-B) and in continuous (Au_xPd_y/TiO_2-C).

oligomerisation to form humins during the induction time.[49] Thus, the actual HMF conversion should not be considered complete until after 120 min of reaction, after which the products of HMF degradation are < 5 % of the total yield.

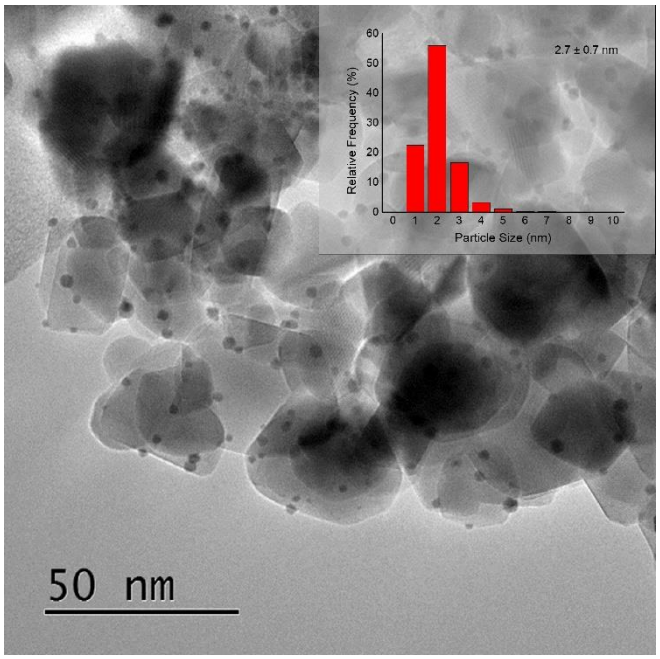

Figure 2. Representative BF-TEM image and (inset) respective particle size distribution of the $Au_{75}Pd_{25}/TiO_2$ catalyst prepared in continuous mode.

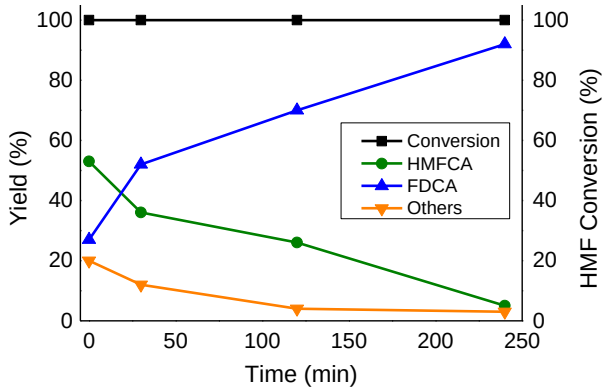

Figure 3. Reaction profile of the HMF oxidation to FDCA using $Au_{75}Pd_{25}/TiO_2$-C. Reaction conditions: temperature 70 °C, O_2 pressure 10 bar, molar ratio HMF/total metal = 100, molar ratio NaOH/HMF = 2.

As described earlier, three AuPd bimetallic catalysts with different nominal metal molar compositions (namely $Au_{75}Pd_{25}$, $Au_{50}Pd_{50}$ and $Au_{25}Pd_{75}$) were synthesised and compared with the monometallic Au and Pd systems for the selective oxidation of HMF to FDCA. The catalytic results for the materials prepared with the continuous flow set-up are reported in Figure 4. Monometallic Pd was the least active of the series: after 4 h of reaction, the conversion of HMF reached only 86 %, while all the Au-based catalysts reached 100 % conversion. In addition, the selectivity towards FDCA of the Pd/TiO_2-C catalyst was very poor, representing only 2 % of the yield after 4 h, while the major product was HMFCA (42 % yield). High fractional amounts of unidentified products were also detected (38 % yield). Interestingly, a small amount of FFCA (3 % yield) was observed with the monometallic Pd catalyst, suggesting that both reaction pathways can occur when this metal alone is employed. The production of FDCA showed a typical volcano plot profile upon the addition of Au to Pd, reaching a maximum at a composition of $Au_{75}Pd_{25}$ (94 % yield), after which the FDCA yield decreased back to lower values (64 % with the monometallic Au/TiO_2-C catalyst).

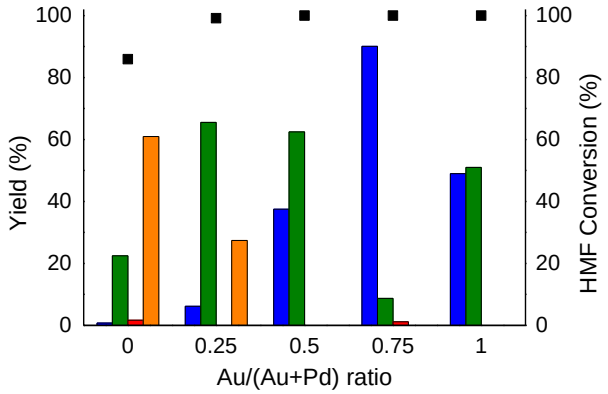

Figure 4. HMF conversion and product yield with the catalysts prepared using continuous flow method. Products: (blue) FDCA, (green) HMFCA, (red) FFCA and (orange) Others. Reaction conditions: temperature 70 °C, time 4 h, O_2 pressure 10 bar, molar ratio HMF/total metal = 100, molar ratio NaOH/HMF = 2.

The same range of AuPd compositions was used for the synthesis of catalysts with the batch technique. The catalytic results for this series of materials are reported in Figure 5. Both activity and selectivity followed the same trend as observed with the continuous route catalysts. The highest yield of FDCA was obtained with $Au_{75}Pd_{25}/TiO_2$-B (90 %), while monometallic Pd/TiO_2-B showed no selectivity towards FDCA and high production of unidentified products. From the direct comparison between the catalysts prepared *via* the batch and continuous methods, it is clear that higher yields of FDCA were always reached with the materials synthesised with the latter technique. This is particularly evident for the $Au_{50}Pd_{50}/TiO_2$-B catalyst, where the FDCA yield increased from 37 % with the batch prepared catalyst to 73 % with its counterpart prepared under continuous flow conditions. We attribute this difference to two concurrent effects, namely a particle size effect and a metal composition effect. The catalysts prepared with the millifluidic set-up in all the cases exhibited smaller nanoparticles and had a more uniform Au-Pd surface composition (Table 2).

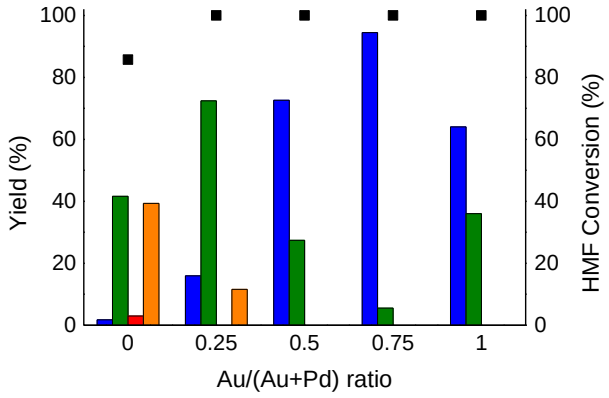

Figure 5. HMF conversion and product yield with the catalysts prepared using the batch method. Products: (blue) FDCA, (green) HMFCA, (red) FFCA and (orange) Others. Reaction conditions: temperature 70 °C, time 4 h, O_2 pressure 10 bar, molar ratio HMF/total metal = 100, molar ratio NaOH/HMF = 2.

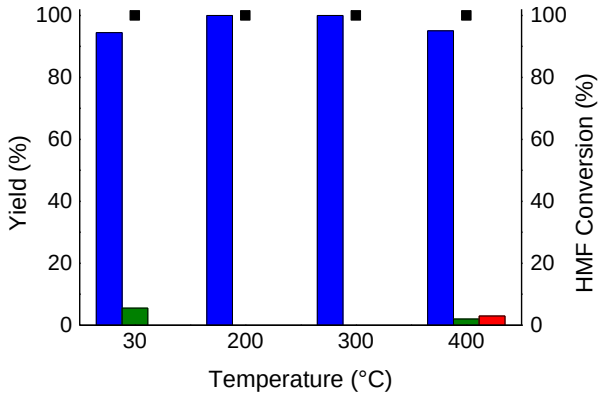

Figure 6. HMF conversion and product yield for the $Au_{75}Pd_{25}/TiO_2$-C catalysts heat treated at different calcination temperatures. Products: (blue) FDCA, (green) HMFCA and (red) FFCA. Reaction conditions: temperature 70 °C, time 4 h, O_2 pressure 10 bar, molar ratio HMF/total metal = 100, molar ratio NaOH/HMF = 2.

Additional thermal treatments were performed on the superior $Au_{75}Pd_{25}/TiO_2$-C catalyst to see if its catalytic performance could be further optimised. These treatments consisted of an initial calcination step in static air at 200, 300 or 400 °C, followed by a reduction step at the same temperature in 5% H_2/N_2 as described in the Experimental Section. These treatments were chosen based on the following facts: (i) to investigate the removal of the protective PVA ligands from the surface of the nanoparticle in order to induce stronger metal-support interactions (SMSI), thus unblocking the desired active sites and (ii) to maintain particle size and metallic oxidation state. The results, presented in Figure 6, show the beneficial effect of performing the thermal treatments at 200 and 300 °C, where > 99 % yield of FDCA was reached in both cases. This small but appreciable increase in yield can be attributed to either the partial removal of PVA ligands caused by the calcination step, and/or the formation of an SMSI.[50] Recent studies, in fact, have demonstrated that SMSI effects can occur even at temperatures as low as 200 °C when TiO_2 is used as a support.[51] A small change in particle size was observed upon thermal treatment with the mean particle diameter increasing from its initial value of 2.7 nm to 3.3 nm and 3.8 nm for the 200 °C and 300 °C calcined samples respectively (Table 3 and Figure S4). The thermal treatment had the additional effect of slightly increasing the concentration of Pd at the surface of the nanoparticles, as observed by XPS analysis (Table S1). The highest temperature treatment of 400 °C, on the other hand, caused the formation of some by-products (*i.e.,* HMFCA and FFCA, with 2 and 3 % yields respectively). We ascribed this detrimental effect to the increase in mean particle size caused by the higher calcination temperature where the mean size, in fact, increased up to 5.5 nm.

Catalyst	Mean particle size (nm)
$Au_{75}Pd_{25}/TiO_2$-C	2.7 ± 0.7
$Au_{75}Pd_{25}/TiO_2$-C-200	3.3 ± 1.0
$Au_{75}Pd_{25}/TiO_2$-C-300	3.8 ± 1.1
$Au_{75}Pd_{25}/TiO_2$-C-400	5.5 ± 1.8
$Au_{75}Pd_{25}/TiO_2$-C-200 - 5th reaction	4.6 ± 1.8

Table 3. Mean particle sizes of the different $Au_{75}Pd_{25}/TiO_2$-C catalysts and thermally treated at different calcination temperatures.

Finally, catalyst reusability tests were carried out on the 200 °C calcined $Au_{75}Pd_{25}/TiO_2$-C catalyst prepared using the continuous flow method (Figure 7). This catalyst showed good stability, maintaining an FDCA yield higher than 99 % for fours usage cycles. After the 4th reaction however, the production of FDCA decreased to 86 %, with a consequent increase in HMFCA and FFCA production (with 9 % and 5 % yields, respectively). TEM analysis showed a significant increase in average particle diameter, from 3.3 nm for the fresh calcined catalyst to 4.6 nm for one used for 5 cycles (Table 3 and Figure S5). Furthermore, the particle size distribution became significantly broader, increasing from ± 1.0 nm to ± 1.8 nm, with the additional presence of some very large AuPd nanoparticles in the 10 – 15 nm range. The particle sintering phenomena are most likely exacerbated, by the lack of PVA stabilising agent on the surface of the nanoparticles due to its partial removal during the thermal treatment step and recycling tests.

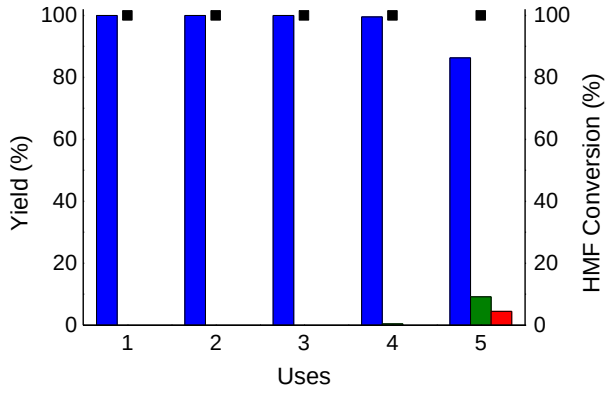

Figure 7. Catalyst reusability tests carried out with the $Au_{75}Pd_{25}/TiO_2$-C catalyst calcined at 200 °C. Products: (blue) FDCA, (green) HMFCA and (red) FFCA. Reaction conditions: temperature 70 °C, time 4 h, O_2 pressure 10 bar, molar ratio HMF/total metal = 100, molar ratio NaOH/HMF = 2.

Conclusions

This study highlights the importance of the materials synthesis procedure adopted in the production of active and highly selective catalyst materials. A series of monometallic Au and Pd and bimetallic AuPd nanoparticles with different Au:Pd ratios were synthesised using a continuous millifluidic approach and deposited onto TiO_2. This technique provides a better control over mean particle size and metal composition compared to traditional batch preparation approaches. To demonstrate this, the as prepared catalysts were compared to similar materials synthesised using a conventional batch technique, namely sol-immobilisation. Through TEM and XPS analysis, the catalysts synthesised using the continuous flow approach showed a smaller particle size and a more uniform Au:Pd composition. These structural differences translated to catalysts, which exhibited higher activity and selectivity in the oxidation of HMF to FDCA, an important precursor used in the production of bio-polymers. The highest FDCA yield (94 %) was obtained with the catalyst prepared using the continuous flow method with a nominal Au:Pd molar composition of 75:25. The yield was further enhanced to > 99 % by exposing the catalyst to a calcination-treatment at 200 °C, followed by a reduction step. This heat treatment protocol had the effect of partially removing the protective PVA ligands used during the nanoparticle synthesis and inducing stronger metal-support interactions. The catalyst proved to be stable in four consecutive reaction runs, although particle sintering started to limit performance during the 5th reaction cycle.

Experimental Section

Materials

Millifluidic reactor – For the millifluidic set-up, a dual channel peristaltic pump (Cole-Parmer Masterflex C/S) was used in combination with Puri-Flex tubing (i.d. = 1.14 mm) and perfluoroalkoxy alkane (PFA) T-shape connections (Swagelok, i.d. = 3.17 mm). A schematic diagram of the millifluidic reactor set-up is shown in Figure S1.

Catalyst synthesis – Hydrogen tetrachloroaurate ($HAuCl_4$, 99.999 %), potassium tetrachloropalladate (K_2PdCl_4, 99.99 %), poly(vinyl alcohol) (PVA, M_w = 9000–10 000, 80 % hydrolysed), sodium borohydride ($NaBH_4$, 99.99 %), titanium dioxide (TiO_2, Degussa P25) and sulphuric acid (H_2SO_4, 95 %) were purchased from Sigma-Aldrich and used without further treatments for the synthesis of our catalyst materials.

5-hydroxymethylfurfural (99.999 %) and NaOH (pellets) were purchased from AvaBiochem and Sigma Aldrich, respectively. Both chemicals were used as received.

Catalyst preparation

Monometallic Au and Pd and bimetallic Au_xPd_y nanoparticles were synthesised with different Au:Pd molar ratios (nominally 25:75, 50:50 and 75:25) and deposited onto a titania powder as support. Two techniques were employed for the catalyst synthesis, a classical batch sol-immobilisation method (denoted Au_xPd_y/TiO_2-B) and a continuous flow millifluidic method (denoted Au_xPd_y/TiO_2-C). In the former method, the metal nanoparticles were formed in batch in a beaker, and the support was added to the colloidal solution in a subsequent step. In the latter technique, the metal nanoparticles were formed continuously inside a millifluidic reactor and the colloid dropped into a suspension of the TiO_2 support.

Batch synthesis – In a typical 1 g synthesis of 1 wt% Au_xPd_y/TiO_2-B catalyst, the requisite amount of metal precursors ($HAuCl_4$ and/or K_2PdCl_4) were added to a beaker containing deionised water in order to obtain the appropriate Au:Pd molar ratio (100:0, 75:25, 50:50, 25:75 and 0:100). Next, 1.2 mL of a 1 wt% polyvinyl alcohol solution (PVA : metal weight ratio = 6:5) was then added under vigorous stirring conditions. To this solution, the appropriate amount of a freshly prepared solution 0.1 mol L^{-1} of $NaBH_4$ was quickly added ($NaBH_4$: metals molar ratio = 5:1). A rapid change in colour indicated the formation of the metallic colloid. After 30 minutes, 0.99 g of support (TiO_2) was added to the beaker, and the suspension was acidified to pH 1 by addition of a few drops of concentrated H_2SO_4. After 1 h, the suspension was filtered, washed thoroughly with 1 L of deionised water and the catalyst dried at 80 °C for 4 h.

Continuous synthesis – The detailed description of the apparatus used is thoroughly described elsewhere[40]. A simplified schematic of the apparatus is presented in Figure S1. In a typical 1 g synthesis of 1 wt% Au_xPd_y/TiO_2-C catalyst, the requisite amount of metal precursors ($HAuCl_4$ and/or K_2PdCl_4) were added to a beaker containing deionised water in order to obtain the appropriate Au:Pd molar ratio (100:0, 75:25, 50:50, 25:75 and 0:100). 1.2 mL of a 1 wt% polyvinyl alcohol solution (PVA: metals weight ratio = 1.2) was then added and the solution stirred for 5 minutes. In a separate beaker, the appropriate amount of a freshly prepared solution 0.1 mol L^{-1} of $NaBH_4$ was diluted in order to have a final $NaBH_4$: metals molar ratio of 5. The two solutions were pumped together using a peristaltic pump through a perfluoroalkoxy alkane (PFA) T-shape connection. The metallic colloid prepared was pumped through a 60 cm length of microbore puri-flex tubing and deposited into a beaker containing 0.99 g of support stirred in 50 mL of slightly acidic deionised water (concentrated H_2SO_4 in order to reach pH 2). After all the metal colloid was immobilised onto the support, the suspension was filtered, washed with 1 L of deionised water and dried at 80 °C for 4 h.

Thermal treatment – High temperature treatments were carried out on the dried catalysts. The procedure consisted of a first calcination step in static air for 3 h at either 200, 300 or 400 °C. The desired temperature was reached with a heating ramp of 10 °C min^{-1}. At the end of the calcination period, H_2 was introduced into the tubular furnace via a 5 % H_2/Ar flow for an additional 3 h. At the end of the treatment, the furnace was cooled down to room temperature and the catalyst collected from the quartz boat and stored in an air-tight glass vial.

Oxidation reactions

The catalytic testing experiments were carried out using an autoclave reactor of 250 mL capacity, equipped with a mechanical stirrer and measurement probes for recording temperature and pressure. The reactor was charged with an aqueous solution (25 mL distilled water) containing 0.1 g of HMF, catalyst (HMF/total metal molar ratio = 100:1) and NaOH (HMF/NaOH molar ratio = 1:2). The autoclave was purged three times with O_2 (5 bar) and then pressurised to the desired working pressure (10 bar). If not indicated otherwise, the temperature was increased to 70 °C and the reaction mixture was stirred at 400 rpm for the indicated reaction time (0.5 - 4 h). The initial time of the reaction (*i.e.,* time zero) was considered when the set point temperature was reached (after ~10 min). At the end of the reaction, the reactor was cooled down to room temperature and the aqueous solution was centrifuged and filtered. Next, the reaction mixture was diluted 10 times before chromatographic analysis was performed. An Agilent Infinity 1260 liquid chromatograph (HPLC-DAD) equipped with an Aminex HPX 87-H 300 mm 7.8 mm column using a 0.005 M H_2SO_4 solution as the mobile phase was used for this analysis. An external calibration method was employed for the identification and quantification of reactants and products using commercial samples as a reference. Carbon loss was calculated through a comparison of converted HMF to the sum of the products formed.

Catalyst characterisation

Transmission Electron Microscopy (TEM) experiments were carried out using a JEOL JEM-2100 electron microscope operating at an accelerating voltage of 200 kV. The catalyst samples were first dispersed in ethanol and sonicated for 5 min. A single drop of the suspension was then deposited onto a 300-mesh carbon-coated copper grid and the solvent allowed to evaporate. Nanoparticles count was performed using ImageJ version 1.52d.

X-ray photoelectron spectroscopy (XPS) measurements were performed using a Thermo Scientific K-α^+ spectrometer. The samples were analysed using a monochromatic Al X-ray source operating at 72 W (6 mA at 12 kV), with the signal averaged over an oval-shaped area of approximately 600 × 400 μm in dimension. Data were recorded at pass energies of 150 eV for survey scans and 40 eV for high resolution scans with a 1.0 eV and 0.1 eV step size, respectively. Charge neutralisation of the sample was achieved using a combination of both low energy electrons and argon ions (less than 1 eV energy) which gave a C1s binding energy of 284.8 eV. All data were analysed using CasaXPS (v2.3.20) using Scofield sensitivity factors and an energy exponent of −0.6.

The metal loading and nominal Au : Pd composition of the catalysts was verified using an Agilent 4100 Microwave Plasma-Atomic Emission Spectrometer (MP-AES). In a typical experiment, 50 mg of sample were suspended in 4 mL of aqua regia, diluted to 50 mL and then left to digest for 16 h. The solution was then filtered to remove the undissolved support material, and the concentration was evaluated against a calibration solution freshly prepared before the analysis.

Acknowledgements

We would like to thank MaxNet Energy for financial support and the Cardiff Electron Microscopy unit for use of facilities.

Keywords: Bimetallic • Gold • Palladium • HMF • Oxidation • FDCA

[1] *BP Statistical Review of World Energy 2018*, **2018**.

[2] J. H. J. Spiertz, F. Ewert, *NJAS - Wageningen J. Life Sci.* **2009**, *56*, 281–300.

[3] D. M. Alonso, S. G. Wettstein, J. A. Dumesic, *Chem. Soc. Rev.* **2012**, *41*, 8075–8098.

[4] S. P. Teong, G. Yi, Y. Zhang, *Green Chem.* **2014**, *16*, 2015–2026.

[5] J. B. Binder, R. T. Raines, *J. Am. Chem. Soc.* **2009**, *131*, 1879–1985.

[6] X. Qi, M. Watanabe, T. M. Aida, R. L. Smith, *Bioresour. Technol.* **2012**, *109*, 224–228.

[7] A. A. Rosatella, S. P. Simeonov, R. F. M. Frade, C. a. M. Afonso, *Green Chem.* **2011**, *13*, 754–793.

[8] K. Gupta, R. K. Rai, S. K. Singh, *ChemCatChem* **2018**, *10*, 2326–2349.

[9] F. Menegazzo, E. Ghedini, M. Signoretto, *Molecules* **2018**, *23*, 1–18.

[10] I. K. M. Yu, D. C. W. Tsang, *Bioresour. Technol.* **2017**, *238*, 716–732.

[11] S. Cattaneo, H. Naslhajian, F. Somodi, C. Evangelisti, A. Villa, L. Prati, *Molecules* **2018**, *23*, 1–13.

[12] A. Jouve, S. Cattaneo, S. Capelli, M. Stucchi, C. Evangelisti, A. Villa, L. Prati, *Molecules* **2019**, *24*, 316–330.

[13] T. Werpy, G. Petersen, A. Aden, J. Bozell, J. Holladay, J. White, A. Manheim, *US Dep. Energy* **2004**, 1–69.

[14] A. J. J. E. Eerhart, A. P. C. Faaij, M. K. Patel, *Energy Environ. Sci.* **2012**, *5*, 6407–6422.

[15] E. de Jong, M. A. Dam, L. Sipos, G.-J. M. Gruter, in *Biobased Monomers, Polym. Mater.*, American Chemical Society, **2012**, pp. 1–13.

[16] W. Partenheimer, V. V. Grushin, *Adv. Synth. Catal.* **2001**,

343, 102–111.

[17] T. Miura, H. Kakinuma, T. Kawano, H. Matshisa, *US7411078*, **2008**.

[18] P. Pal, S. Saravanamurugan, *ChemSusChem* **2019**, *12*, 145–163.

[19] H. Xia, S. Xu, H. Hu, J. An, C. Li, *RSC Adv.* **2018**, *8*, 30875–30886.

[20] F. A. Kucherov, L. V. Romashov, K. I. Galkin, V. P. Ananikov, *ACS Sustain. Chem. Eng.* **2018**, *6*, 8064–8092.

[21] L. Hu, L. Lin, Z. Wu, S. Zhou, S. Liu, *Renew. Sustain. Energy Rev.* **2017**, *74*, 230–257.

[22] F. Neaţu, R. S. Marin, M. Florea, N. Petrea, O. D. Pavel, V. I. Pârvulescu, *Appl. Catal. B Environ.* **2016**, *180*, 751–757.

[23] S. E. Davis, L. R. Houk, E. C. Tamargo, A. K. Datye, R. J. Davis, *Catal. Today* **2011**, *160*, 55–60.

[24] Z. Zhang, J. Zhen, B. Liu, K. Lv, K. Deng, *Green Chem.* **2015**, *17*, 1308–1317.

[25] G. Yi, S. P. Teong, Y. Zhang, *Green Chem.* **2016**, *18*, 979–983.

[26] Z. Zhang, K. Deng, *ACS Catal.* **2015**, *5*, 6529–6544.

[27] D. Bonincontro, A. Lolli, A. Storione, A. Gasparotto, B. Berti, S. Zacchini, N. Dimitratos, S. Albonetti, *Appl. Catal. A Gen.* **2019**, 117279.

[28] X. Wan, C. Zhou, J. Chen, W. Deng, Q. Zhang, Y. Yang, Y. Wang, *ACS Catal.* **2014**, *4*, 2175–2185.

[29] O. Casanova, S. Iborra, A. Corma, *ChemSusChem* **2009**, *2*, 1138–1144.

[30] B. N. Zope, R. J. Davis, *Green Chem.* **2011**, *13*, 3484–3491.

[31] A. Villa, M. Schiavoni, S. Campisi, G. M. Veith, P. Laura, *ChemSusChem* **2013**, *6*, 609–612.

[32] A. Lolli, S. Albonetti, L. Utili, R. Amadori, F. Ospitali, C. Lucarelli, F. Cavani, *Appl. Catal. A Gen.* **2015**, *504*, 408–419.

[33] D. Bonincontro, A. Lolli, A. Villa, L. Prati, N. Dimitratos, G. M. Veith, L. E. Chinchilla, G. A. Botton, F. Cavani, S. Albonetti, *Green Chem.* **2019**, *21*, 4090–4099.

[34] S. Albonetti, A. Lolli, V. Morandi, A. Migliori, C. Lucarelli, F. Cavani, *Appl. Catal. B Environ.* **2015**, *163*, 520–530.

[35] S. Cattaneo, M. Stucchi, A. Villa, L. Prati, *ChemCatChem* **2019**, *11*, 309–318.

[36] B. Siyo, M. Schneider, M.-M. Pohl, P. Langer, N. Steinfeldt, *Catal. Letters* **2014**, *144*, 498–506.

[37] R. Schenk, V. Hessel, N. Jongen, V. Buscaglia, S. Guillement-Fritsch, A. G. Jones, *Encycl. Nanosci. Nanotechnol.* **2004**, *7*, 287–296.

[38] J. DeMello, A. DeMello, *Lab Chip* **2004**, *4*, 11–15.

[39] A. Villa, D. Wang, D. S. Su, L. Prati, *Catal. Sci. Technol.* **2015**, *5*, 55–68.

[40] S. Cattaneo, S. Althahban, S. Freakley, M. Sankar, T. Davies, Q. He, N. Dimitratos, C. Kiely, G. J. Hutchings, *Nanoscale* **2019**, *11*, 8247–8259.

[41] T. Pasini, M. Piccinini, M. Blosi, R. Bonelli, S. Albonetti, N. Dimitratos, J. A. Lopez-Sanchez, M. Sankar, Q. He, C. J. Kiely, et al., *Green Chem.* **2011**, *13*, 2091–2099.

[42] S. Albonetti, T. Pasini, A. Lolli, M. Blosi, M. Piccinini, N. Dimitratos, J. A. Lopez-Sanchez, D. J. Morgan, A. F. Carley, G. J. Hutchings, et al., *Catal. Today* **2012**, *195*, 120–126.

[43] M. Brust, M. Walker, D. Bethell, D. J. Schiffrin, R. Whyman, *J. Chem. Soc. Chem. Commun.* **1994**, 801–802.

[44] L. Prati, A. Villa, *Catalysts* **2012**, *2*, 24–37.

[45] L. Prati, G. Martra, *Gold Bull.* **1999**, *32*, 96–101.

[46] N. Dimitratos, J. A. Lopez-Sanchez, J. M. Anthonykutty, G. Brett, A. F. Carley, R. C. Tiruvalam, A. A. Herzing, C. J. Kiely, D. W. Knight, G. J. Hutchings, *Phys. Chem. Chem. Phys.* **2009**, *11*, 4952–4961.

[47] S. Cattaneo, S. J. Freakley, D. J. Morgan, M. Sankar, N. Dimitratos, G. J. Hutchings, *Catal. Sci. Technol.* **2018**, *8*, 1677–1685.

[48] Y. Lee, Y. Jeon, *J. Korean Phys. Soc.* **2000**, *37*, 451–455.

[49] S. Albonetti, A. Lolli, V. Morandi, A. Migliori, C. Lucarelli, F. Cavani, *Appl. Catal. B Environ.* **2015**, *163*, 520–530.

[50] J. A. Lopez-Sanchez, N. Dimitratos, C. Hammond, G. L. Brett, L. Kesavan, S. White, P. Miedziak, R. Tiruvalam, R. L. Jenkins, A. F. Carley, et al., *Nat. Chem.* **2011**, *3*, 551–556.

[51] Y. Li, Y. Fan, H. Yang, B. Xu, L. Feng, M. Yang, Y. Chen, *Chem. Phys. Lett.* **2003**, *372*, 160–165.

Entry for the Table of Contents

FULL PAPER

Continuous flow synthesis of bimetallic AuPd catalysts and their application in the selective oxidation of 5-hydroxymethylfurfural to 2,5-furandicarboxylic acid

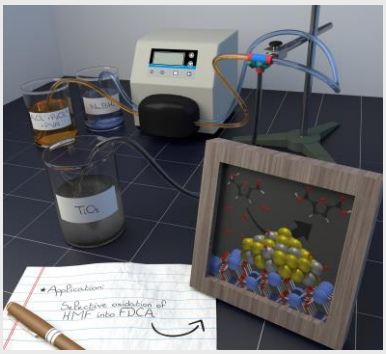

Stefano Cattaneo,[a][b] Danilo Bonincontro,[c] Takudzwa Bere,[a] Christopher J. Kiely,[a][d] Graham J. Hutchings,[a] Nikolaos Dimitratos[a][c] and Stefania Albonetti*[c]*

Page No. – Page No.

Continuous flow synthesis of bimetallic AuPd catalysts for the selective oxidation of 5-hydroxymethylfurfural to 2,5-furandicarboxylic acid